

Mechano-chemistry stability and water effect on gas selectivity in mixed-metals Zeolitic Imidazole Frameworks: A systematic investigation from van der Waals corrected density functional theory

*Diem Thi-Xuan Dang,^{*a} Huong Thi-Diem Nguyen,^b Nam Thoai,^c Jer-lai Kuo,^d Nhung Tuyet Thi Nguyen,^e and Duc Nguyen-Manh^f*

Supporting Information

^aCenter for Innovative Materials and Architectures (INOMAR), Vietnam National University - Ho Chi Minh City, Ho Chi Minh City 721337, Vietnam; ^bFaculty of Chemistry, University of Science, Vietnam National University – Ho Chi Minh City, Ho Chi Minh City 721337, Vietnam; ^cHigh Performance Computing Lab and Faculty of Computer Science & Engineering, University of Technology, Vietnam National University - Ho Chi Minh City, Ho Chi Minh City 721337, Vietnam; ^dInstitute of Atomic and Molecular Sciences, Academia Sinica, Taipei 10617, Taiwan; ^eDepartment of Chemistry, School of Education, Can Tho University, Can Tho City 900000, Vietnam; ^fCulham Center for Fusion Energy, United Kingdom Atomic Energy Authority, OX14 3DB, United Kingdom.

(E-mail of corresponding authors: xuandiemdang@gmail.com, dxdiem@inomar.edu.vn)

Table of Contents

Page	Contents
S2	Section S1: metal-imidazolate-metal
S4	Section S2: Computational details
S6	Section S3: Structure information
S9	Section S4: Mechanical stability
S13	Section S5: Electronic structures
S20	Section S6: Charge density differences
S23	Section S7: Nudged elastic band

Section S1: Metal – imidazolate - Metal

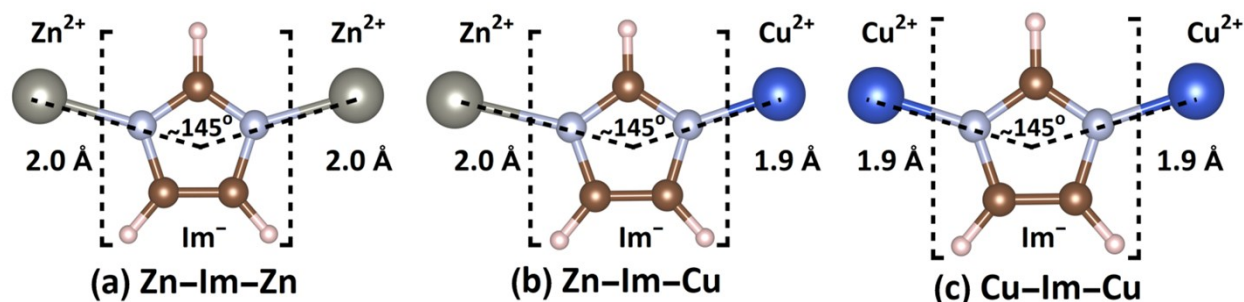


Figure S1. The angles and bondings of (a) Zn-im-Zn, (b) Zn-im-Cu and (c) Cu-im-Cu linkages. Zn - gray, Cu - blue, N - light blue, C - brown, H - light pink.

The ZIF structures are similar to zeolitic SiO₂ since the angle metal-im-metal is the same (ca. 135–145°) as the Si-O-Si angle. Therefore, these materials share many advantages of zeolite chemistry such as the remarkable chemical and thermal stability. In the crystal structure of ZIF materials, we find that metal-im-metal angles are different for different metals. Clearly, the metal has an impact on the values of the metal-im-metal angles. In order to understand this effect, we replaced different metals and measured various metal-im-metal angles. Since there are no available crystal structures for these metals, we have considered them as clusters. Metal-im-metal cluster is optimized in a box of 25 Å in length with different metal pairs. The calculated together with literature results are summarized in Table S5. The angle with two different metals is smaller than the same metal M1-im-M2 < M1-im-M1, M1-im-M2 < M2-im-M2. As an example, Zn-im-Zn and Cu-im-Zn angles are 146.20° and 144.60°, while Zn-im-Cu angle is 148.70°. Nonetheless, as considered in the crystal, this rule is no longer true and metal-im-metal angles range from 135 to 140°. Moreover, the metal-nitrogen bondings range from 1.83 – 2.29 Å.

Table S1. The data of M_1 -im- M_2 angle and bond length of M_1 -Nitrogen, M_2 -Nitrogen. Here, M_1 , M_2 are metals and M_1 -im- M_2 are clusters.

M_1 -im- M_2	Source	M_1 -im- M_2 angle ($^\circ$)	N-C-N angle ($^\circ$)	d_{M_1-N} (\AA)	d_{M_2-N} (\AA)	Reference
V-im-V	Cluster	142.80	112.63	2.04	2.04	This work
Ti-im-Ti	Cluster	145.70	113.02	2.08	2.08	This work
V-im-Ti	Cluster	146.20	112.82	2.02	2.07	This work
Fe-im-Fe	Cluster	142.00	111.71	1.97	1.97	This work
Fe-im-V	Cluster	141.00	112.26	1.99	2.04	This work
Fe-im-Ti	Cluster	140.10	112.38	2.03	2.06	This work
Co-im-Co	Cluster	143.40	111.52	1.81	1.85	This work
Co-im-Zn	Cluster	144.50	111.91	1.83	2.42	This work
Co-im-Cu	Cluster	141.70	111.57	1.84	1.87	This work
	$[\text{Co}^{\text{II}}\text{Cu}^{\text{I}}_2(\text{Im})_4]_\infty$	140.38	111.72	1.99	1.87	[1]
Zn-im-Zn	Cluster	146.20	111.57	2.10	2.11	This work
	ZIF-1	135.08	112.64	2.02	2.02	[2]
	ZIF-2	136.27	112.57	2.02	2.02	[3]
Cu-im-Cu	Cluster	144.60	111.47	1.87	1.87	This work
	ZIF-204	137.51	111.47	2.00	1.98	[4]
Zn-im-Cu	Cluster	148.70	111.49	2.29	1.84	This work
Zn-im-Cu (ion Cu^+)	ZIF-202	140.63	113.13	1.99	1.87	[4]
Zn-im-Cu (ion Cu^{2+})	ZIF-204	140.64 135.62	112.10	2.00	2.04	[4]

Section S2: Computational details

The lines of the high symmetry points used in band structure calculations are Z (0, 0, 0.5) – A (0.5, 0.5, 0.5) – M (0.5, 0.5, 0) – G (0, 0, 0) – Z (0, 0, 0.5) – R (0, 0.5, 0.5) – X (0, 0.5, 0) – G (0, 0, 0) for ZIF-202; L (0.5, 0, 0.5) – M (0.5, 0.5, 0.5) – A (0, 0, 0.5) – G (0, 0, 0) – Y (0.5, 0.5, 0) – V (0.5, 0, 0) – L (0.5, 0, 0.5) for ZIF-203; and G (0, 0, 0) – B (0, 0, 0.5) – A (-0.5, 0, 0.5) – Y (0.5, 0, 0) – G (0, 0, 0) – Z (0, 0.5, 0) – D (0, 0.5, 0.5) – E (-0.5, 0.5, 0.5) – C (0.5, 0.5, 0) for ZIF-204 and ZIF-204 (hydrated).

Lenard-Jones 6-12 terms of potential combined with Coulomb electrostatic potential

$$U(r_{ij}) = 4\epsilon_{ij} \left[\left(\frac{\sigma_{ij}}{r_{ij}} \right)^{12} - \left(\frac{\sigma_{ij}}{r_{ij}} \right)^6 \right] + \frac{1}{4\pi\epsilon_0} \frac{q_i q_j}{r_{ij}}, \quad (1)$$

where ϵ_0 is the dielectric constant of vacuum, r_{ij} is the distance between atom i and atom j , q_i is the partial electric charge of atom i .

The parameters ϵ_{ij} and σ_{ij} are respectively the depth and the diameter of Lenard-Jones potential well, and these are totally determined via Lorentz-Berthelot mixing rules³⁸ given as follows

$$\epsilon_{ij} = \sqrt{\epsilon_i \epsilon_j}, \sigma_{ij} = \frac{1}{2}(\sigma_i + \sigma_j). \quad (2)$$

Table S2. The Lennard-Jones force field parameters for ZIF-204, ZIF-204 (hydrated 3.5 wt%), ZIF-204 (hydrated 1.8 wt%) and ZIF-204 (hydrated 6.8 wt%) from UFF and DREIDING force fields, and the ones for CO₂ and CH₄ from TraPPE force field. The charges of the framework were taken from Bader charge in PBE method.

Atom	$\epsilon/k_B(K)$	$\sigma (\text{\AA})$	$q (e^-)$			
			ZIF-204	ZIF-204 (hydrated 3.5 wt%)	ZIF-204 (hydrated 1.8 wt%)	ZIF-204 (hydrated 6.8 wt%)
ZIF-Zn	62.400	2.460	0.577	1.199	1.011	0.974
ZIF-Cu	2.516	3.114	0.949	0.981	0.794	0.912
ZIF-N	38.949	3.263	-0.801	-0.880	-0.853	-0.864
ZIF-C	47.856	3.473	0.527	0.516	0.564	0.568
ZIF-H	7.649	2.846	-0.127	-0.106	-0.138	-0.138
C_co2	27.000	2.800	0.700	0.700	0.700	0.700
O_co2	79.000	3.050	-0.350	-0.350	-0.350	-0.350
CH4_sp3	148.000	3.730	0.000	0.000	0.000	0.000
O_water	76.542	3.150	-	0.442	0.343	0.423
H_water	0.000	0.000	-	-0.906	-0.811	-0.918

CO₂ is modeled as a rigid linear triatomic molecule with three charged Lennard-Jones interaction sites located at each atom with C=O bond length 1.20 Å. CH₄ is modeled by the united-atom model, in which it is treated as a single interaction center with its efficient potential.

By the definition of Kubelka-Munk function i.e.

$$F(R) = \frac{\alpha}{S} = \frac{(1-R)^2}{2R}, \quad (3)$$

whereas R is diffused reflectance of the sample, it can be seen that Kubelka-Munk function is directly proportional to absorption coefficient α and inversely proportional to scattering coefficient S .

Section S3: Structure Information

Table S3. Some optimized average bond length (Å) and bond angles (°) for ZIF-202, ZIF-203 (solvents), ZIF-203, ZIF-204 (solvents), ZIF-204 and ZIF-204 (hydrated 3.5 wt%) at their equilibrium volumes.

Materials		Zn-N (Å)	Cu1-N (Å)	Cu2-N (Å)	Zn-im-Cu1 (°)	Zn-im-Cu2 (°)	Cu1-im-Cu2 (°)
ZIF-202	Exp.	1.99	1.87		140.63		-
	PBE	2.00	1.86		141.10		-
	PBE-D3	1.98	1.86		140.94		-
ZIF-203 (solvents)	Exp.	1.99	2.00	2.00	137.00	141.00	139.40
	PBE	2.00	2.00	1.99	136.12	143.08	137.23
	PBE-D3	1.99	1.98	1.98	139.84	140.76	135.18
ZIF-203	PBE	2.00	1.99	1.99	142.50	141.80	139.80
	PBE-D3	2.00	1.98	1.98	141.10	134.40	135.53
ZIF-204 (solvents)	Exp.	2.00	2.01	2.01	140.64	135.62	137.51
	PBE	1.99	2.03	2.00	139.83	138.42	138.85
	PBE-D3	1.99	2.02	1.98	132.37	130.45	137.08
ZIF-204	PBE	2.00	1.99	1.99	141.50	141.60	140.40
	PBE-D3	1.99	1.98	1.98	137.10	138.80	135.60
ZIF-204 (hydrated 3.5 wt%)	PBE	2.00	1.99	1.99	140.20	140.20	140.30
	PBE-D3	1.99	1.99	1.99	136.00	132.70	138.90

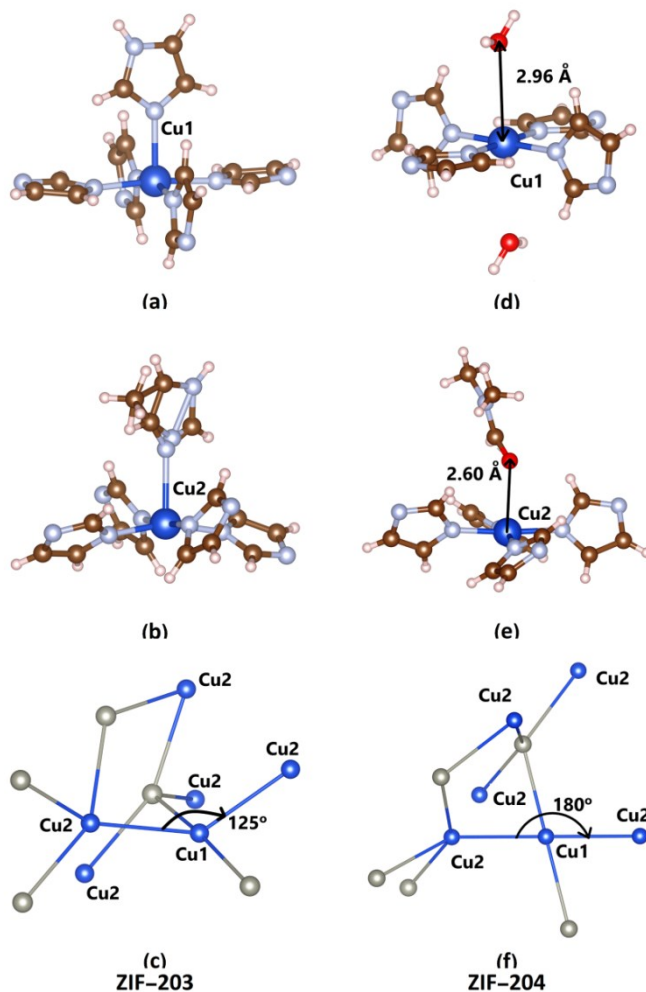


Figure S2. The networks surrounding Cu1, Cu2 and the metal nodes distribution of (a), (b), (c) ZIF-203 and (d), (e), (f) ZIF-204. In ZIF-203 (solvents), Cu atoms adopt a square pyramidal geometry with imidazolates occupying the in-plane coordination sites. A free imidazole is located at the axial site for Cu1 atom while disordered ligand (both MeCN and im partially occupy) for Cu2 atoms. For ZIF-204 (solvents), each Cu1 atom has octahedral coordination with two coordinatively unsaturated (open) site toward pores that can hold two H₂O molecules. Each Cu2 atom adopts a square pyramidal geometry with the axial site being coordinated by a dimethylformamide (DMF) solvent ligand. For these ZIFs, the adjacent metal nodes interact with one Zn node via imidazoles are one Cu1 and three Cu2 nodes. Similarly, those for one Cu1 node are two Zn and two Cu2 nodes; those for one node Cu2 are three Zn and one Cu1 node. The disparity between ZIF-203 and -204 is Cu2-Cu1-Cu2 angle is 125° and 180°, respectively. Zn - gray, Cu - blue, N - light blue, C - brown, H - light pink and O - red.

Table S4. Six possible combinations of MeCN and im with four Cu₂ atoms in ZIF-203 (solvents).

Case	Cu ₂ (first)	Cu ₂ (second)	Cu ₂ (third)	Cu ₂ (fourth)
1	im	im	MeCN	MeCN
2	MeCN	im	im	MeCN
3	MeCN	MeCN	im	im
4	im	MeCN	im	MeCN
5	im	MeCN	MeCN	im
6	MeCN	im	MeCN	im

Table S5. The optimized structures and energy data for ZIF-203 (solvents) in six cases in which the case 3 and 6, the calculations were not converged.

Case	Methods	a (Å)	b (Å)	c (Å)	α	β	γ	E (eV)
1	PBE	13.13	13.25	20.27	108.52	108.24	57.02	-1418.69
	PBE-D3	12.61	12.59	20.54	108.95	108.89	56.51	-1433.62
2	PBE	13.15	13.25	20.29	108.78	108.45	57.12	-1418.66
	PBE-D3	12.70	12.65	20.54	109.59	109.18	55.98	-1433.70
3	PBE	x	x	x	x	x	x	x
	PBE-D3	x	x	x	x	x	x	x
4	PBE	13.26	12.98	20.14	107.94	107.56	57.79	-1418.39
	PBE-D3	12.65	12.43	20.39	108.70	108.89	58.23	-1433.50
5	PBE	13.14	13.25	20.31	108.78	108.49	56.93	-1418.62
	PBE-D3	12.69	12.67	20.53	109.59	109.17	55.89	-1433.72
6	PBE	x	x	x	x	x	x	x
	PBE-D3	x	x	x	x	x	x	x

Section S4: Mechanical Stability

Table S6. The eigenvalues of stiffness tensor of ZIF-202, -203, -203 (solvents), -204 and -204 (3.5 wt% hydrated) in PBE and PBE-D3 method. All eigenvalues of tensor are positive meaning that the material is mechanically stable.

		The eigenvalues of stiffness tensor	Satisfy the mechanical stability?
ZIF-202	PBE	6.79, 9.71, 9.71, 10.75, 32.31, 67.13	Yes
	PBE-D3	11.57, 14.77, 15.73, 15.73, 39.10, 91.12	Yes
ZIF-203	PBE	2.34, 3.45, 4.79, 5.96, 8.93, 47.50	Yes
	PBE-D3	-3.94, -0.66, 3.24, 4.19, 7.15, 45.92	No
ZIF-203 (solvents)	PBE	2.77, 4.23, 4.92, 6.94, 9.74, 38.30	Yes
	PBE-D3	2.12, 4.24, 5.00, 7.64, 9.64, 45.48	Yes
ZIF-204	PBE	0.37, 0.69, 5.94, 6.58, 8.95, 41.18	Yes
	PBE-D3	0.06, 0.86, 5.90, 7.39, 7.59, 46.95	Yes
	PBE-D3+U	24.32, 225.75, 2173.81, 11655.27, 31046.35, 48897.61	Yes
ZIF-204 (3.5 wt% hydrated)	PBE	0.02, 0.31, 4.22, 6.97, 9.11, 37.49	Yes
	PBE-D3+U	9.93, 72.31, 1143.84, 5459.36, 33512.03, 96148.16	Yes

The bulk and shear moduli in the Voigt-Reuss-Hill approximation are given by

$$B = (B_V + B_R)/2, G = (G_V + G_R)/2, \quad (4)$$

where B_V and G_V correspond to Voigt's bulk modulus and shear modulus, B_R and G_R are Reuss's bulk modulus and shear modulus, respectively, and they are for tetragonal crystal structure given by⁵

$$B_V = [2(C_{11} + C_{12}) + C_{33} + 4C_{13}]/9, \quad (5)$$

$$G_V = (4C_{11} - 2C_{12} - 4C_{13} + 2C_{33} + 12C_{44} + 6C_{66})/30, \quad (6)$$

$$B_R = [(C_{11} + C_{12})C_{33} - 2C_{13}^2]/(C_{11} + C_{12} + 2C_{33} - 4C_{13}), \quad (7)$$

$$G_R = 15\{2[2(C_{11} + C_{12}) + C_{33} + 4C_{13}]/[(C_{11} + C_{12})C_{33} - 2C_{13}^2] + 6/(C_{11} - C_{12}) + 6/C_{44} + 3/C_{66}\}^{-1}, \quad (8)$$

and

$$B_V = [C_{11} + C_{22} + C_{33} + 2(C_{12} + C_{13} + C_{23})]/9, \quad (9)$$

$$G_V = [C_{11} + C_{22} + C_{33} + 3(C_{44} + C_{55} + C_{66}) - (C_{12} + C_{13} + C_{23})]/15, \quad (10)$$

$$B_R = \Omega[a(C_{11} + C_{22} - 2C_{12}) + b(2C_{12} - 2C_{11} - C_{23}) + c(C_{15} - 2C_{25}) + d(2C_{12} + 2C_{23} - C_{13} - 2C_{22}) + 2e(C_{25} - C_{15}) + f]^{-1}, \quad (11)$$

$$G_R = 15\{4[a(C_{11} + C_{22} + C_{12}) + b(C_{11} - C_{12} - C_{23}) + c(C_{15} + C_{25}) + d(C_{22} - C_{12} - C_{23} - C_{13}) + e(C_{15} - C_{25})] + f + g\} \quad (12)$$

for monoclinic crystal structure with

$$a = C_{33}C_{55} - C_{35}^2,$$

$$b = C_{23}C_{55} - C_{25}C_{35},$$

$$c = C_{13}C_{35} - C_{15}C_{33},$$

$$d = C_{13}C_{55} - C_{15}C_{35},$$

$$e = C_{13}C_{25} - C_{15}C_{23},$$

$$f = C_{11}(C_{22}C_{55} - C_{25}^2) - C_{12}(C_{12}C_{55} - C_{15}C_{25}) + C_{15}(C_{12}C_{25} - C_{15}C_{22}) + C_{25}(C_{23}C_{35} - C_{25}C_{33}),$$

$$g = C_{11}C_{22}C_{33} - C_{11}C_{23}^2 - C_{22}C_{13}^2 - C_{33}C_{12}^2 + 2C_{12}C_{13}C_{23},$$

$$\Omega = 2[C_{15}C_{25}(C_{33}C_{12} - C_{13}C_{23}) + C_{15}C_{35}(C_{22}C_{13} - C_{12}C_{23}) + C_{25}C_{35}(C_{11}C_{23} - C_{12}C_{13})] - [C_{15}^2(C_{22}C_{33} - C_{23}^2) + gC_{55}].$$

Further, the Young's modulus (E) and Poisson's ratio (ν) are estimated by⁶

$$E = 9BG/(3B + G), \nu = (3B - 2G)/(6B + 2G) \quad (13)$$

Table S7. The checking the Born criterion for mechanical stability of tetragonal crystal structure of ZIF-202.

These criterion is given by Ref. [5]. Stick \odot means satisfy, cross \rightarrow means unsatisfy.

Born criteria for tetragonal	PBE	PBE-D3
$(C_{11} - C_{12}) > 0$	32.31 \odot	39.10 \odot
$(C_{11} + C_{33} - 2C_{13}) > 0$	42.18 \odot	47.39 \odot
$[2(C_{11} + C_{12}) + C_{33} + 4C_{13}] > 0$	181.59 \odot	261.96 \odot

Table S8. The checking the Born criterion for mechanical stability of monoclinic crystal structure of ZIF-203 and ZIF-203 (solvents). These criterion is given by Ref. [5]. Stick ✨ means satisfy, cross → means unsatisfy.

Born criteria for monoclinic	ZIF-203		ZIF-203 (solvents)	
	PBE	PBE-D3	PBE	PBE-D3
$[C_{11} + C_{22} + C_{33} + 2(C_{12} + C_{13} + C_{23})] > 0$	122.42 ✨	96.55 ✨	102.55 ✨	122.75 ✨
$(C_{33}C_{55} - C_{35}^2) > 0$	164.18 ✨	138.90 ✨	131.45 ✨	196.41 ✨
$(C_{44}C_{66} - C_{46}^2) > 0$	15.08 ✨	6.38 ✨	17.87 ✨	15.11 ✨
$(C_{22} + C_{33} - 2C_{23}) > 0$	22.26 ✨	18.88 ✨	20.90 ✨	21.91 ✨
$[C_{22}(C_{33}C_{55} - C_{35}^2) + 2C_{23}C_{25}C_{35} - C_{23}^2C_{55} - C_{25}^2C_{33}] > 0$	1159.47 ✨	333.21 ✨	984.24 ✨	1703.20 ✨
$\{2[C_{15}C_{25}] > 0$	7686.87 ✨	-934.86 →	9457.4 ✨	12962 ✨

Table S9. The checking the Born criterion for mechanical stability of monoclinic crystal structure of ZIF-204 and ZIF-204 (hydrated 3.5 wt%). These criterion is given by Ref. [5]. Stick \odot means satisfy, cross \rightarrow means unsatisfy.

Born-Huang criteria for monoclinic	ZIF-204			ZIF-204 (hydrated 3.5 wt%)	
	PBE	PBE-D3	PBE-D3+U	PBE	PBE-D3+U
$[C_{11} + C_{22} + C_{33} + 2(C_{12} + C_{13} + C_{23})] > 0$	108.01 \odot	115.86 \odot	119.61	97.06 \odot	72.84 \odot
$(C_{33}C_{55} - C_{35}^2) > 0$	34.61 \odot	45.55 \odot	58.54 \odot	86.51 \odot	149.63 \odot
$(C_{44}C_{66} - C_{46}^2) > 0$	2.46 \odot	0.45 \odot	8.44 \odot	0.13 \odot	13.69 \odot
$(C_{22} + C_{33} - 2C_{23}) > 0$	15.91 \odot	14.58 \odot	13.97 \odot	10.20 \odot	20.28 \odot
$[C_{22}(C_{33}C_{55} - C_{35}^2) + 2C_{23}C_{25}C_{35} - C_{23}^2C_{55} -$	149.03 \odot	204.59 \odot	491.83 \odot	547.70 \odot	1051.13 \odot
$\left. \begin{matrix} \{2\} \\ > 0 \end{matrix} \right\}$	1503.59 \odot	1802.11 \odot	5790.42 \odot	453.72 \odot	7021.42 \odot

Section S5: Electronic structures

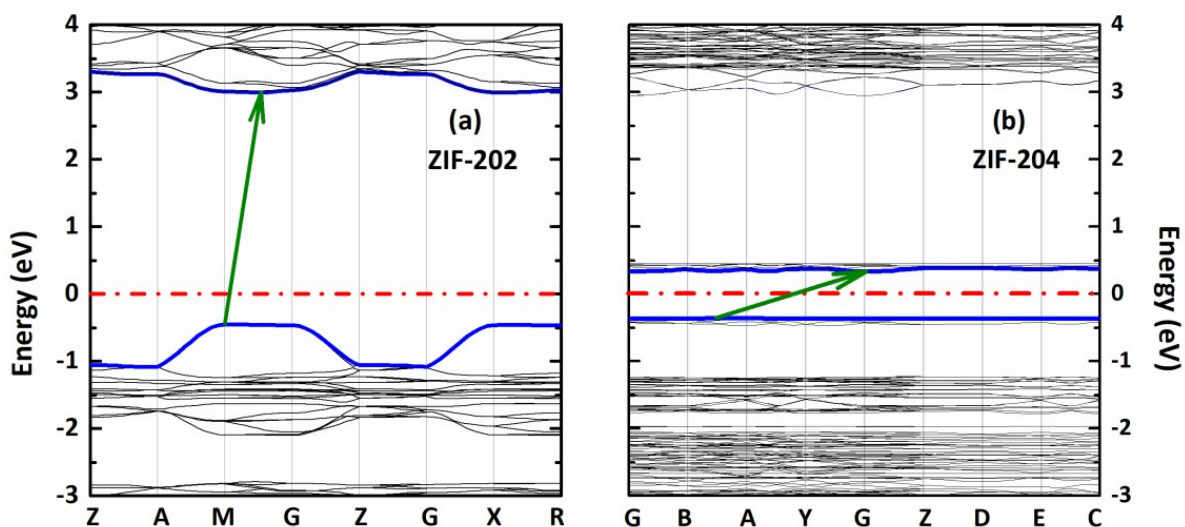


Figure S3. The band structure of (a) ZIF-202, and (b) ZIF-204 from $-3 - 4 eV$ in PBE-D3 method. The Fermi level is set to zero. The blue lines represent the valence and conduction band edges. The arrows represent the transitions from valence band edge to conduction band edge.

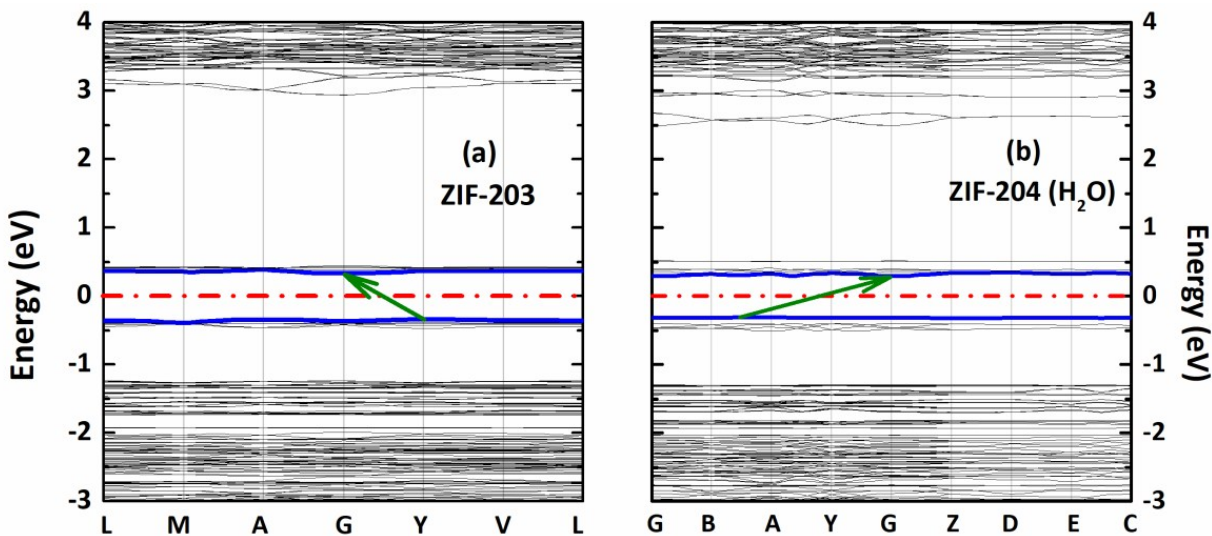


Figure S4. The band structure of (a) ZIF-203 and (b) ZIF-204 (3.5 wt% hydrated) from $-3 - 4 eV$ in PBE method. The Fermi level is set to zero. The blue lines represent the valence and conduction band edges. The arrows represent the transitions from valence band edge to conduction band edge.

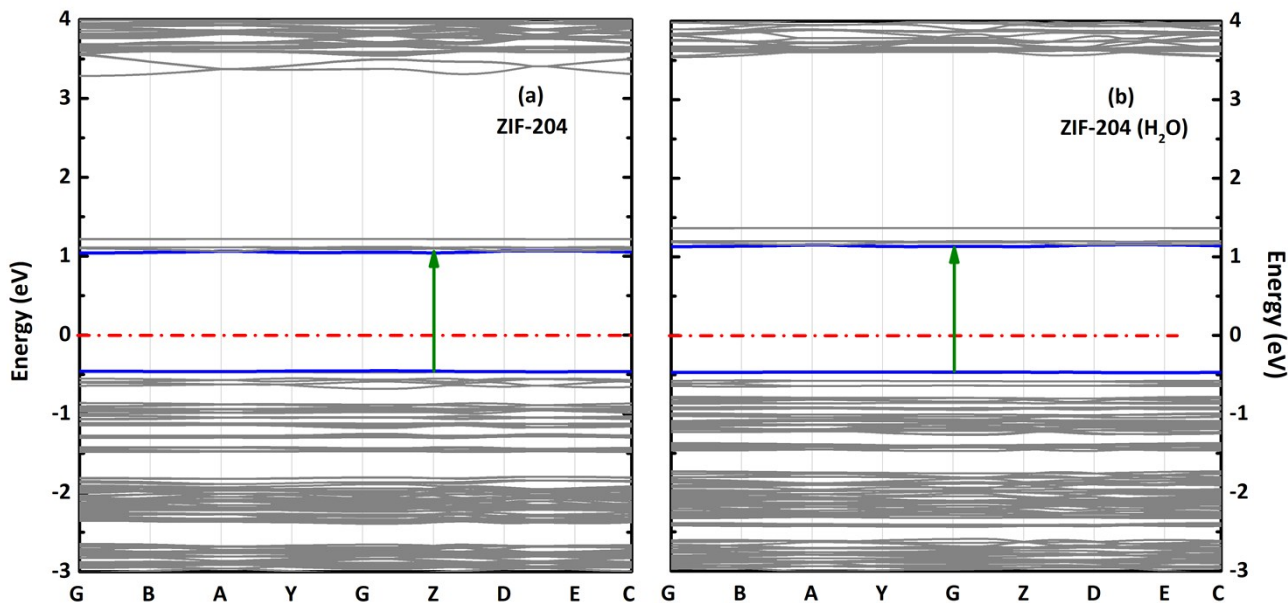


Figure S5. The band structure of (a) ZIF-204 and (b) ZIF-204 (3.5 wt% hydrated) from $-3 - 4 eV$ in PBE-D3+U method. The Fermi level is set to zero. The blue lines represent the valence and conduction band edges. The arrows represent the transitions from valence band edge to conduction band edge.

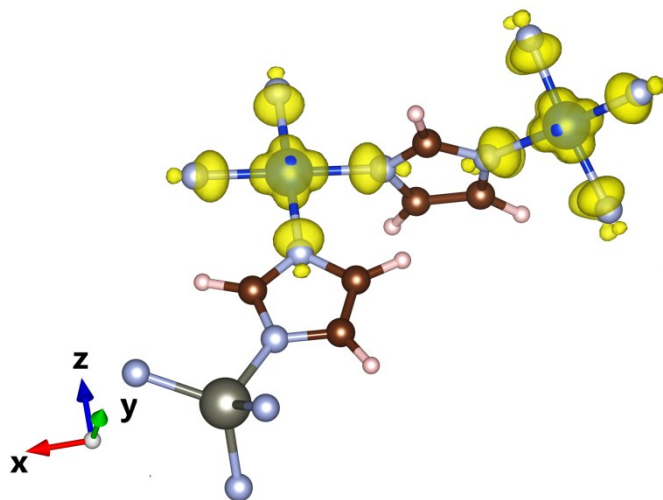


Figure S6. The HOMO of ZIF-204 in PBE-D3 method. The Fermi level is set to zero. Zn - gray, Cu - blue, N - light blue, C - brown, and H - light pink.

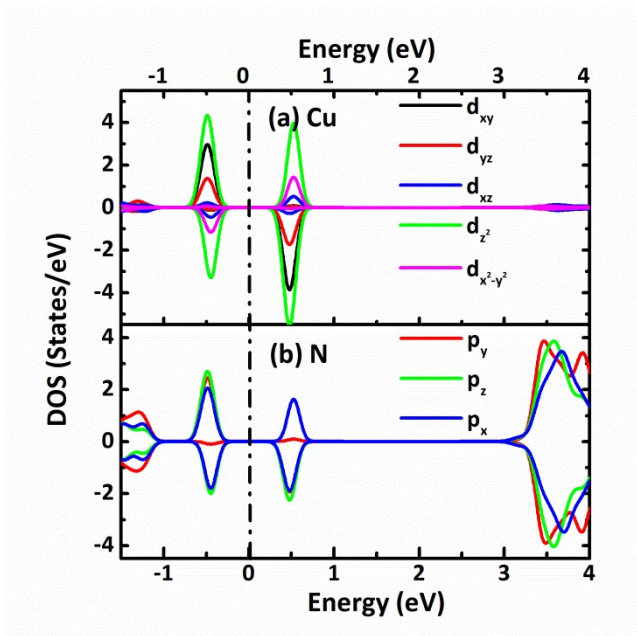


Figure S7. The project density of states of copper d-states and nitrogen p-states for ZIF-204 in PBE-D3 method.

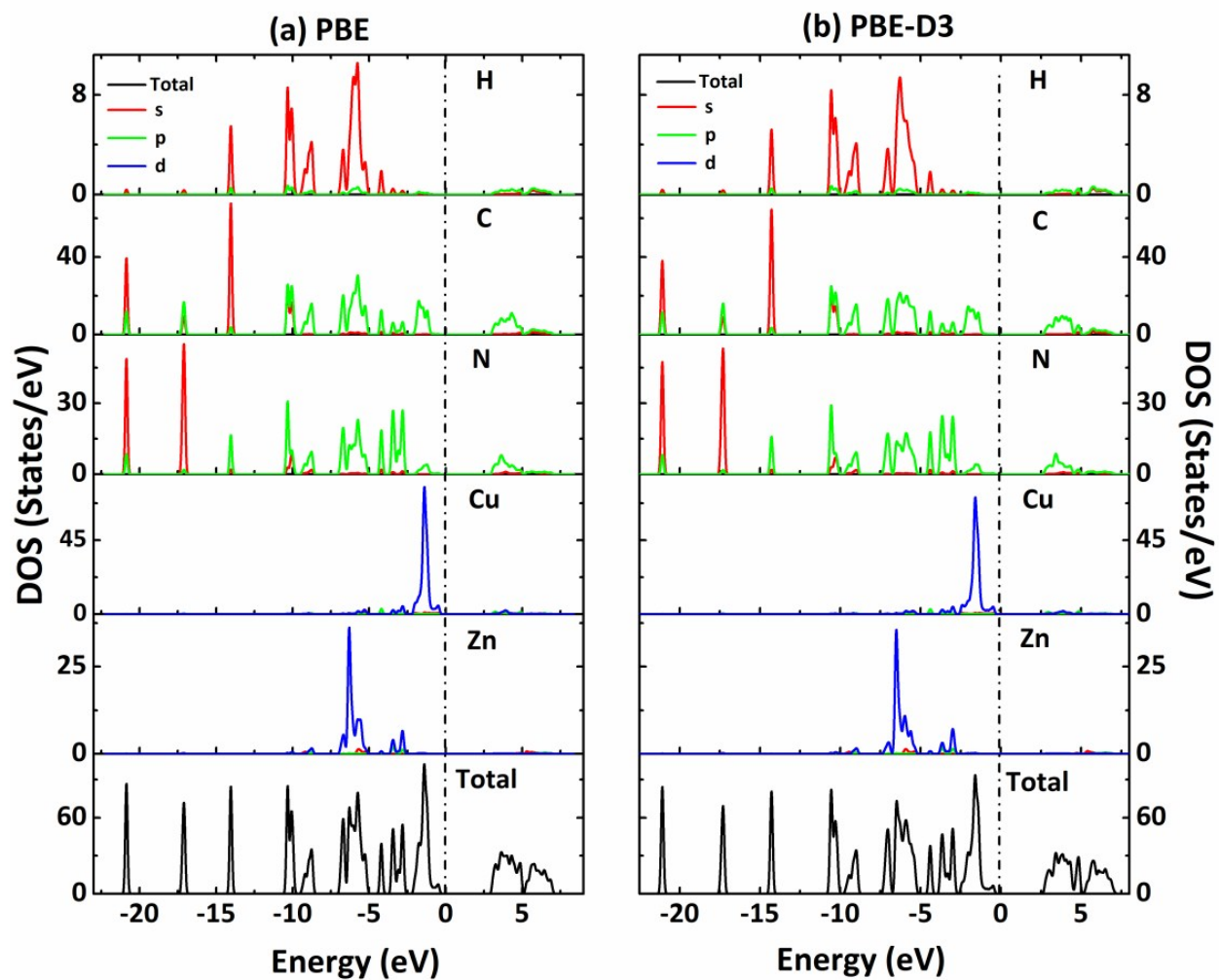


Figure S8. The total density of states and projected density of states for ZIF-202 in (a) PBE and (b) PBE-D3 method. Fermi level is set to zero.

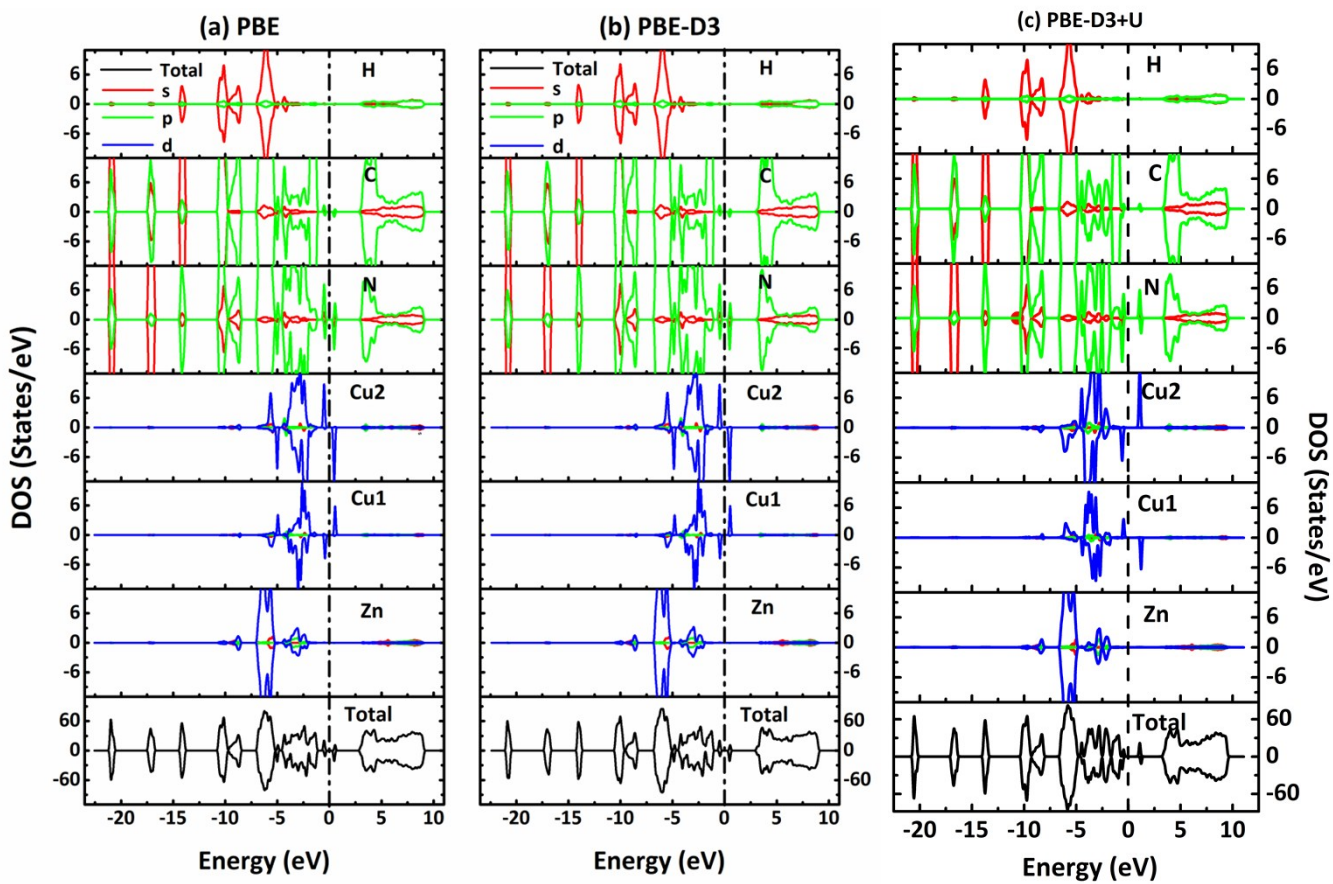


Figure S9. The total density of states and projected density of states for ZIF-204 in (a) PBE, (b) PBE-D3 and (c) PBE-D3+U method. Fermi level is set to zero.

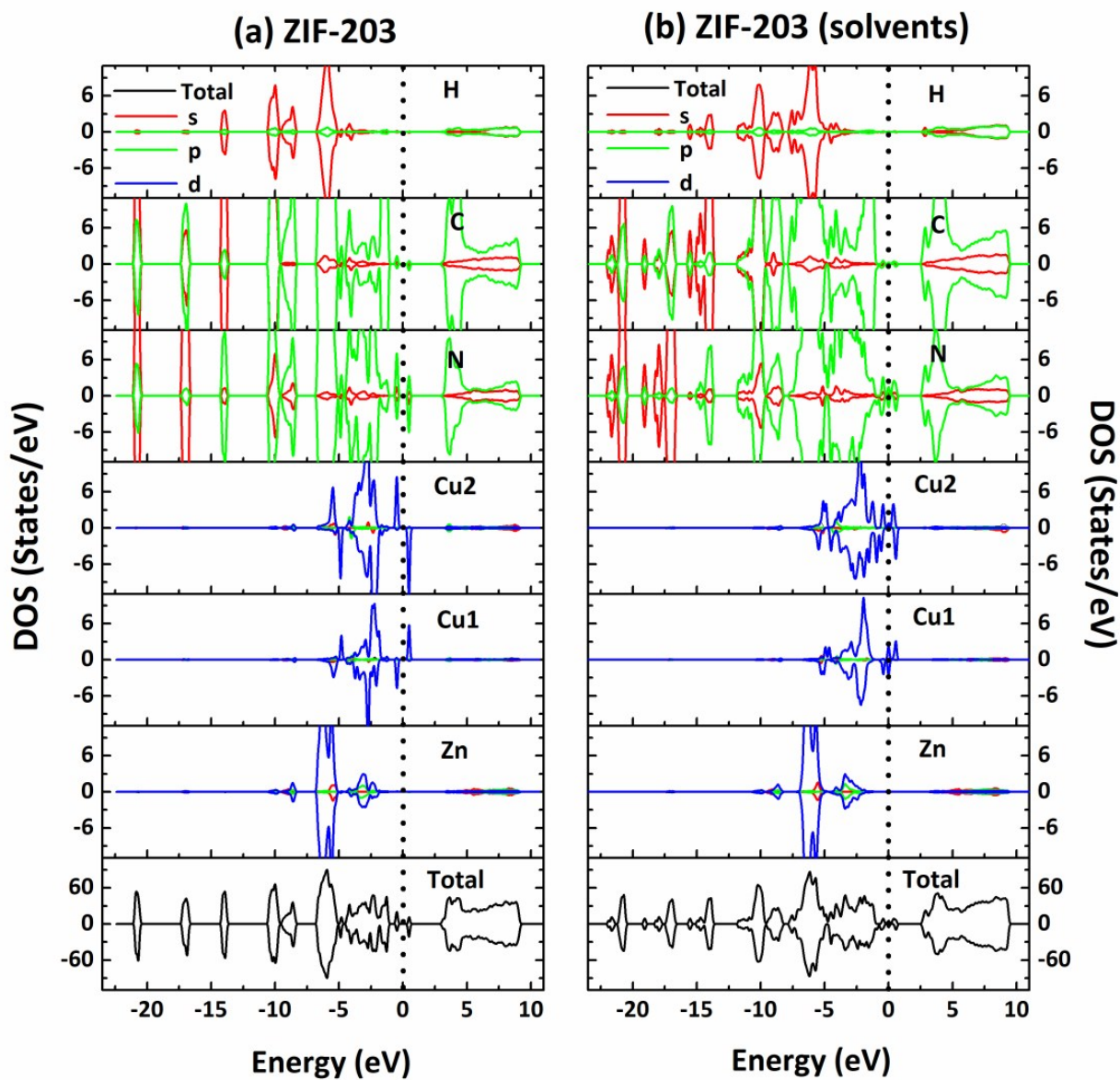


Figure S10. The total density of states and projected density of states for (a) ZIF-203 and (b) ZIF-203 (solvents) in PBE method. Fermi level is set to zero.

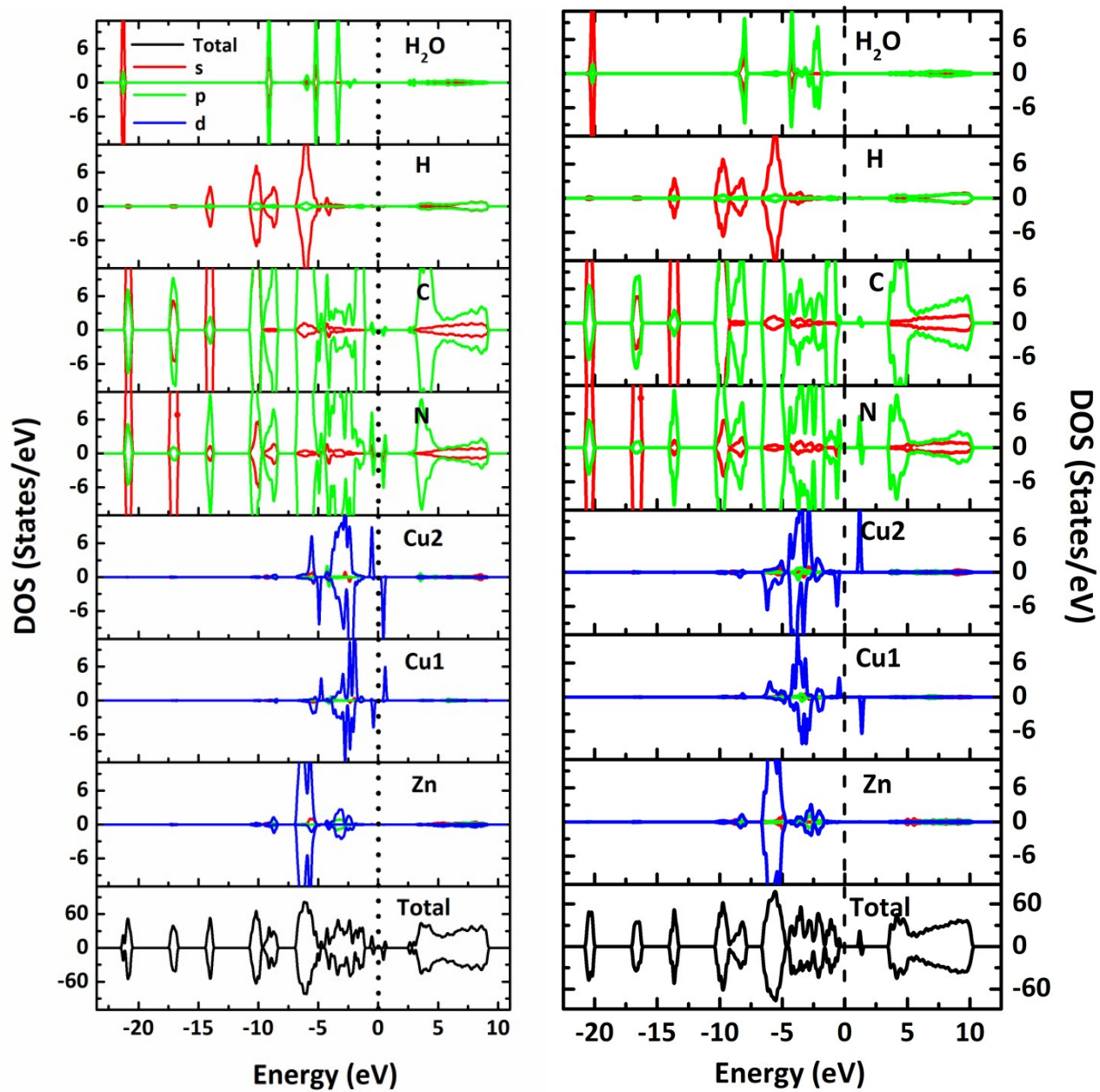


Figure S11. The total density of states and project density of states for ZIF-204 (3.5 wt% hydrated) in (a) PBE and (b) PBE-D3+U method. Fermi level is set to zero.

Section S6: Charge density differences

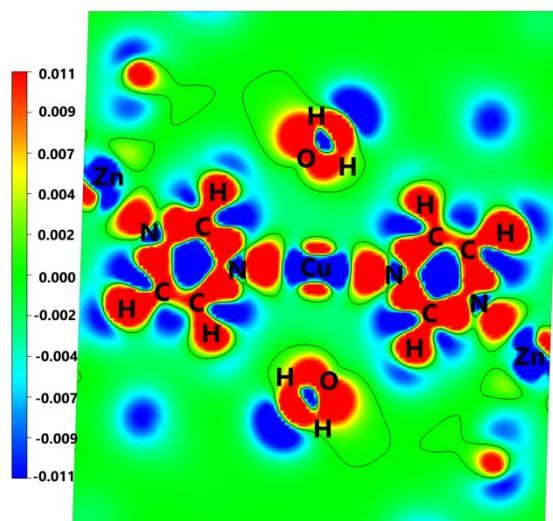


Figure S12. The 2D plot of charge density difference of ZIF-204 (3.5 wt% hydrated) from -0.011 to $0.011 e/\text{\AA}^3$ in PBE method.

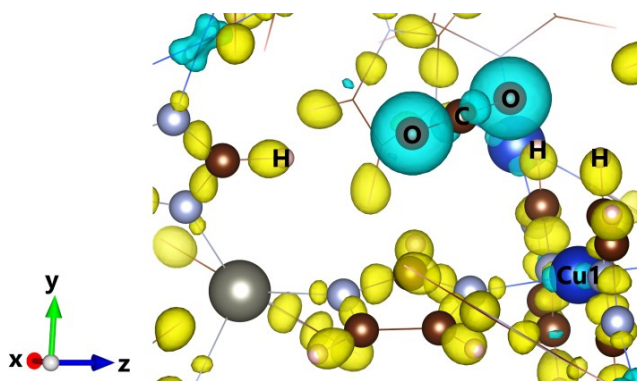
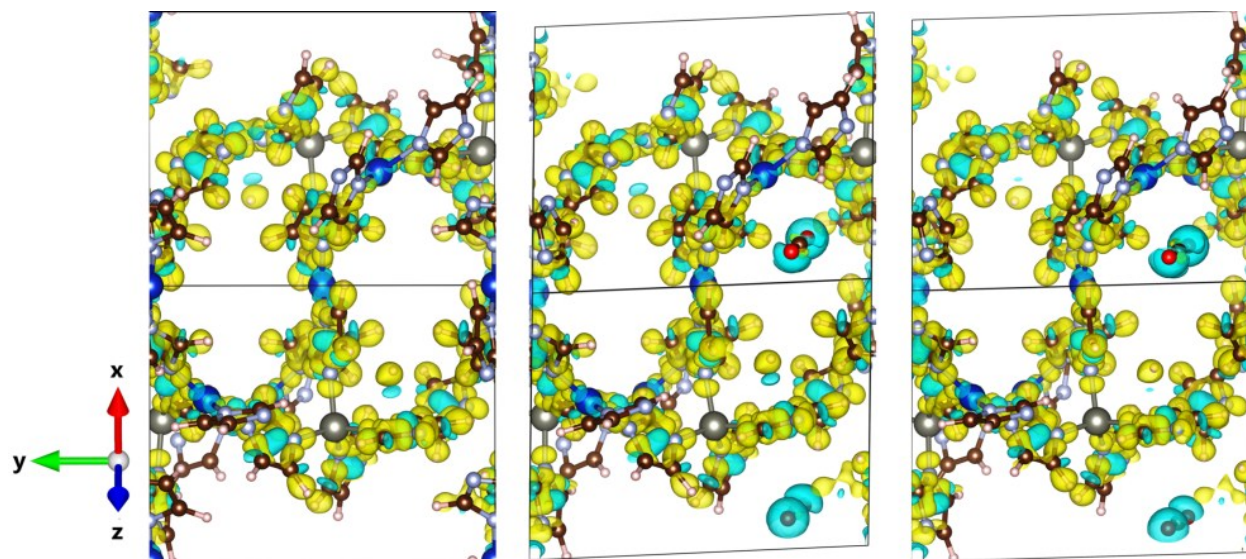


Figure S13. The charge density difference of the complex CO₂/ZIF-204 with Site 1 in PBE-D3 method. The blue isosurfaces are $-50 me/\text{\AA}^3$ and the yellow isosurfaces are $50 me/\text{\AA}^3$.



(a) ZIF-204 in PBE-D3 (b) CO₂/ZIF-204 in PBE-D3 (c) CO₂/ZIF-204 in PBE

Figure S14. The charge density difference of (a) ZIF-204 in PBE-D3 method and the complex CO₂/ZIF-204 (b) in PBE-D3 and (c) PBE method (Site 1). The blue isosurfaces are $-20\text{meV}/\text{\AA}^3$ and the yellow isosurfaces are $20\text{meV}/\text{\AA}^3$. Zn - gray, Cu - blue, N - light blue, C - brown, H - light pink and O - red.

For a more intuitionistic picture of the interaction between the two interacting parts, we have drawn the charge density difference plot of the CO₂/ZIF-204 complex using PBE-D3 in the most stable form in Figure S12. The plot shows the vdW interaction between O (CO₂) with H (ZIF-204). We also carry out a Bader charge analysis by PBE-D3 to prove this judgment. Our results show that the O atom has a net charge of $-0.81 e$, while the nearest H atom has a net positive charge of $0.12 e$.

The charge density difference of ZIF-204 in PBE-D3 is also shown in Figure S13 for comparison. It can be seen from the figure that charge density difference of ZIF-204 seem to have minimal changes when CO₂ is absorbed on the pore. This also gives us another fact that the interaction between CO₂ and ZIF-204 is a weak interaction and the two parts get close to each other with no chemical effect. We have also optimized the complex without the dispersion force and find that the closest contact distance becomes about 3.20\AA . Without the dispersion force, CO₂ is unlikely to be absorbed on the pore stability. In this regard, PBE gives positive binding energies for most sites, while PBE-D3 method predicts negative binding energies, which emphasizes the importance of including dispersion in calculations of gas adsorption on ZIFs.

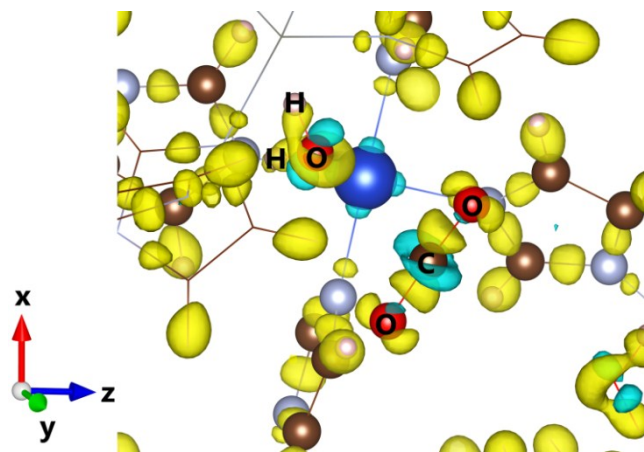


Figure S15. The charge density difference of the complex CO₂/ZIF-204 (3.5 wt% hydrated) with Site 1 in PBE method. The blue isosurfaces are $-50 \text{ me}/\text{\AA}^3$ and the yellow isosurfaces are $50 \text{ me}/\text{\AA}^3$.

We have drawn the charge density difference plot of the CO₂/ZIF-204 (3.5 wt% hydrated) complex using PBE in the most stable form in Figure S14. The plot depicts that the negative charge is mainly located on O (H₂O) which has a large electrostatic attraction with C (CO₂). We also carry out a Bader charge analysis by PBE to prove this judgment. Our results show that the O atom has a net charge of $-0.88 e$, while C atom has a positive charge of $1.47 e$.

Section S7: Nudged elastic band

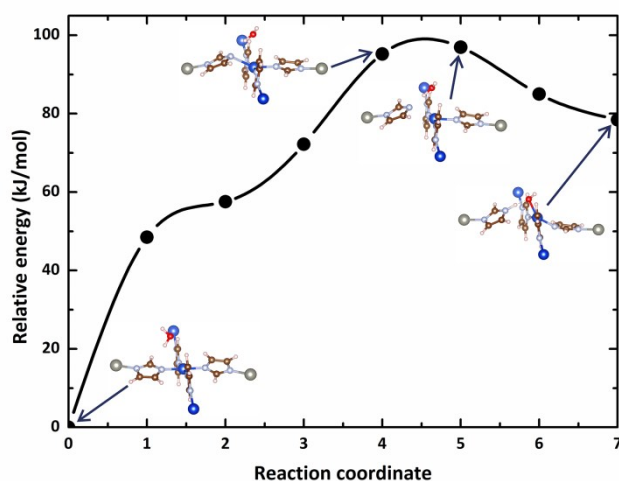


Figure S16. The energy barrier of the dissociative of the water molecule and ZIF-204 in PBE-D3 method. In first stage, the water molecule is separated relatively distal from Cu1 cation with the distance of O (water) and Cu1 (ZIF-204) being 3.53 \AA and H atom oriented towards N anion with the distance of H (water) and N (ZIF-204) being 2.20 \AA . The Cu-N bond is then broken as shown in the transition state while water approaches Cu1 cation with the distance of O (water) and Cu1 (ZIF-204) being 2.42 \AA and H atom is very close to the N atom of imidazole with a distance of 1.26 \AA . Then, there is a dissociation of H_2O and H^+ bonds with the N atom of the imidazole ring. In the final stage, hydroxyl OH^- is bound to the Cu1 position. The energy difference between the initial and final states is 78.41 kJ/mol ; therefore, the final stage is less stable, i.e. both the breakdown of Cu-N and water dissociation destabilize the system.

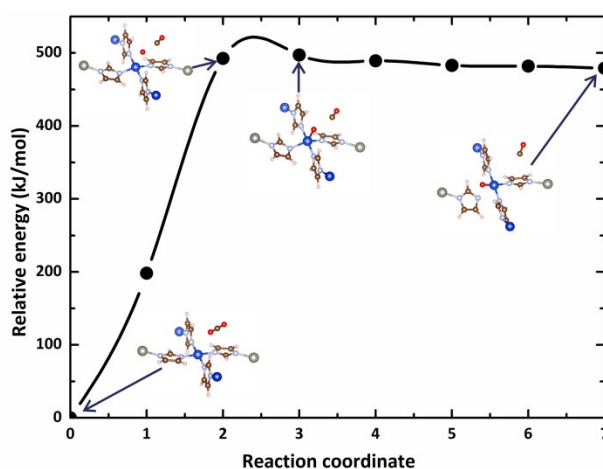


Figure S17. The energy barrier of the dissociative of the CO_2 molecule and ZIF-204 in PBE-D3 method.

At first, the CO_2 molecule is separated relatively distal from Cu1 cation with the distance of O (CO_2) and Cu (ZIF-204) being 3.35 \AA . The C-O bond (CO_2) is then broken and produce CO as shown in the transition state while O (CO_2) approaches Cu1 cation with the distance of O and Cu (ZIF-204) being 2.65 \AA . In the final stage, the Cu-N bond is then broken.

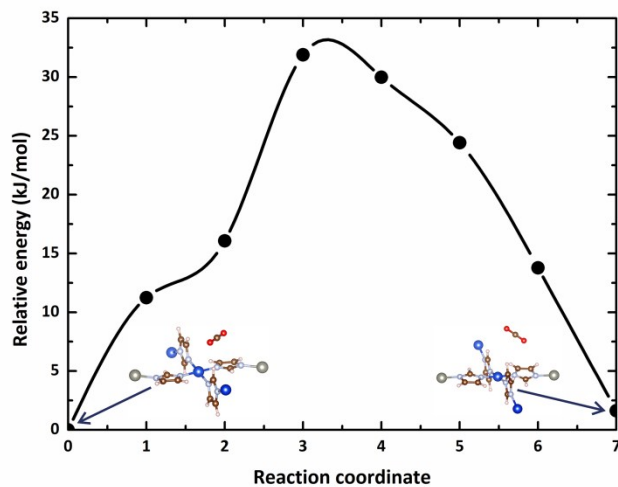


Figure S18. The energy barrier of the migration of the CO₂ molecule in ZIF-204 in PBE-D3 method.

REFERENCES

1. F. Ragot, S. Belin, B. G. Ivanov, D. L. Perry, M. Ortega, T. V. Ignatova, I. G. Kolobov, E. A. Masalitin, G. V. Kamarchuk, A. V. Yermenko, P. Mokinie, J. Wery and E. Faulques, *Mater. Sci.*, 2002, **20**, 13.
2. A. Phan, C. J. Doonan, F. J. Uribe-Romo, C. B. Knobler, M. O’Keeffe and O. M. Yaghi, *Acc. Chem. Res.*, 2010, **43**, 58.
3. D. Banerjee, A. Phan, C. Knobler, H. Furukawa, M. O’Keeffe and O. Yaghi, *Science*, 2008, **319**, 939.
4. N. T. T. Nguyen, T. N. H. Lo, J. Kim, H. T. D. Nguyen, T. B. Le, K. E. Cordova and H. Furukawa, *Inorg. Chem.*, 2016, **55**, 6201.
5. Z. Wu, E. Zhao, H. Xiang, X. Hao, X. Liu, and J. Meng, *Phys. Rev. B*, 2007, **76**, 054115.
6. R. Hill, *Proc. Phys. Soc. A*, 1952, **65**, 349.